PHYSICAL REVIEW A VOLUME 23, NUMBER 3 MARCH 1981

# Optical Hanle effect

V. P. Kaftandjian
*Département des Interactions Moléculaires, Université de Provence, Centre St. Jérôme, 13397 Marseille Cedex 4, France*

C. Delsart and J. C. Keller
*Laboratoire Aimé Cotton,* C.N.R.S. II, Bâtiment 505, 91405 Orsay Cedex, France*
(Received 24 April 1980)

The optical Hanle effect (light-shift-induced zero-field level crossing) has been investigated theoretically and experimentally. In the case of a $J = 0 \rightarrow 1 \rightarrow 0$ three-level system and of a $J = 0 \rightarrow 1$ two-level system, the resonance line shape has been obtained using a nonlinear-response-function method. Approximate expressions, valid under the conditions for the observation of light shifts, are obtained and compared with exact calculations as well as with the corresponding expression for the magnetic Hanle effect. As concerns the weak laser beam which produces the coherent excitation of atomic substates, we have calculated the linear response in the limiting case of monochromatic and of broad-band excitation. The experimental investigation has been performed for the Ba resonance line using two cw dye lasers at $\lambda = 5535$ Å and an atomic beam. The absorption- and dispersion-shaped level crossing resonances have been observed, for narrow- and broad-band excitation, by varying the power of the strong nonresonant laser beam. We have checked that the line shapes are only dependent upon the reduced variable $P_L/\delta$ ($P_L$: beam power; $\delta$: frequency detuning). Using the theoretical expressions, we have tried to fit the experimental curves. Provided that the Gaussian distribution of the beams is taken into account, we have obtained a good agreement between theory and experiment for the whole set of experimental data.

## I. INTRODUCTION

Zero-field level-crossing resonances have been obtained for the first time by Hanle in 1924 through the observation of the magnetic depolarization of the fluorescence light induced by a conveniently polarized source.[1] With broad-band excitation and magnetic-field scanning, the Hanle effect has been extensively studied and applied to lifetimes and relaxation rate measurements for atomic and molecular species.[2] The use of laser sources for the coherent excitation of the Zeeman sublevels has recently led to the observation of strongly modified level-crossing curves. The modifications are related either to the high power density (nonlinear effects), to the monochromaticity, or to both characteristics of laser light.[3,4]

A second kind of zero-field level-crossing effect has been demonstrated in 1926 by Hanle: A static electric field and the quadratic Stark effect replaces the static magnetic field and the Zeeman effect to lift the magnetic substates degeneracy.[5] The fundamental point to observe the resonance is to shift at least one of the sublevels by an externally applied and adjustable effect. It has been recently proposed to use for this purpose the ac Stark effect produced by a nonresonant and powerful laser beam (light shift).[6] The experimental evidence for this "optical Hanle effect" has been obtained in 1979 for the resonance line of barium ($J = 0 \rightarrow J = 1$ two-level system).[7]

Let us consider a collection of atoms with two levels $b$ ($J = 1$, upper level) and $c$ ($J = 0$, lower level) excited by a light source with coherent $\sigma$ polarization (linear polarization perpendicular to the quantization axis $Oz$) so that a Hertzian coherence $\rho_{b_+b_-}$ is created in the excited state $b$. This coherence exhibits a resonant behavior versus the energy distance $\Delta E_{b_+b_-}$ between the sublevels $b_+$ and $b_-$. This level-crossing resonance is usually observed through the polarization characteristics of the fluorescence light by applying a static magnetic field along $Oz$ and varying the strength of the field (magnetic Hanle effect) [Fig. 1(a)]. The resonance curve is centered at zero magnetic field (zero-field level crossing) and its width is proportional to the reciprocal of the lifetime of the upper state. An analogous effect is obtained in a three-level system $a(J = 0) \rightarrow b \rightarrow c$ when a circularly polarized and intense laser field is applied, slightly off resonant relative to the $a \rightarrow b$ transition [Fig. 1(b)]. The oscillating optical electric-field shifts the $b_+$ sublevel by an amount $\Delta E_{b_+b_-} = \Delta = -\beta_2^2/\delta_2$ (optical light shift),[8] $2\beta_2$ is the Rabi nutation frequency for the $b^+ \rightarrow a$ transition, and $\delta_2$ is the frequency detuning. The energy difference $\Delta E_{b_+b_-}$ can be tuned by varying the power $P_L$ of the nonresonant laser ($\beta_2^2 \propto P_L$).

The ac Stark shift can also be produced by a second light field slightly detuned from the $b \rightarrow c$ transition itself (two-level system) [Fig. 1(c)]. The main difference with the previous case is the shift of the lower level which is important in the case of monochromatic excitation. Indeed, the case of monochromatic excitation (monochromatic

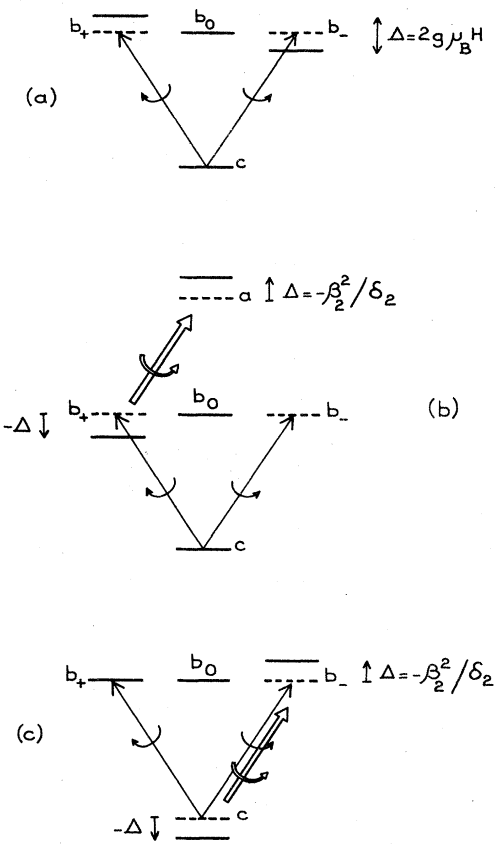


FIG. 1. Level scheme and laser polarizations for the observation of zero-field level crossing. (a) Magnetic Hanle effect, (b) optical Hanle effect (three-level system), (c) optical Hanle effect (two-level system).

laser beam for fluorescence excitation +atomic beam) produces additional features in the level-crossing curve due to the fact that the excitation beam becomes more or less nonresonant when the shift of the levels occurs. The way through which the latter effect appears, differs for the different cases illustrated in Fig. 1. In the above discussion, we have considered the analog of the magnetic Hanle effect, i.e., a circular polarization for the strong field which produces the ac Stark shift ("Faraday" geometry); the use of linear polarization at 45° from one another for the weak excitation beam and for the strong beam ("Kerr" geometry) would give rise to the analog of the electric Hanle effect.[5,6(b)] The expressions Faraday geometry and Kerr geometry refer to the possibility to observe, for the transmission of the weak beam, the optical Faraday effect or the optical Kerr effect induced by the strong beam in a vapor using the particular polarization setting.[9,10]

The theory of the optical Hanle effect is developed in Sec. II, first for the three-level case, and then for the two-level case; narrow-band excitation as well as broad-band excitation are considered and a comparison is made with the magnetic Hanle effect in both cases. The experimental investigation of the effect is presented in Sec. III; particular attention is paid to the experimental divergences from the ideal experiment. The final part of the section is devoted to the quantitative comparison between experimental results and theory.

## II. THEORY OF THE OPTICAL HANLE EFFECT

Let us consider first the geometrical and polarization characteristics of the system (Fig. 2). The atomic beam ($Ox$ direction) is illuminated at right angle by two laser beams counterpropagating along $Oz$ (quantization axis). The weak field $\vec{E}_1$ is resonant and linearly polarized and the strong field $\vec{E}_2$ is nonresonant and circularly polarized. The interaction of the weak field with the atoms [$c(J=0) \rightarrow b(J=1)$ transition] induces some fluorescence light which is detected in the $Oy$ direction. The intensity of the fluorescence emitted from level $b(J=1)$ depends upon the density matrix $\rho$ of the atomic sample in the following way:

$$L_F(\alpha) \propto \rho_{b_+b_-} + \rho_{b_-b_-} - 2\cos 2\alpha\, \mathrm{Re}(\rho_{b_+b_-}) + 2\sin 2\alpha\, \mathrm{Im}(\rho_{b_+b_-}), \quad (1)$$

$\alpha$ is the angle between the $\vec{E}_1$ field polarization direction and the $x$ axis. From an experimental point of view it is possible, using a rotating polarization technique, to measure separately the absorption part $S_A = -2\,\mathrm{Re}(\rho_{b_+b_-})$ and the dispersion part $S_D = +2\,\mathrm{Im}(\rho_{b_+b_-})$ of the coherent contribution to the fluorescence signal; the remaining contribution $S_I = \rho_{b_+b_+} + \rho_{b_-b_-}$ is usually referred as to the incoherent part of the signal.[11] In the following, most of the calculations will thus

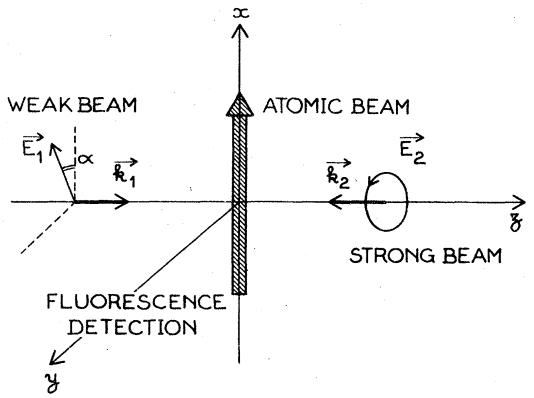


FIG. 2. Geometrical arrangement for the observation of the optical Hanle effect.

be restricted to the determination of the Hertzian coherence $\rho_{b_+b_-}$.

The elements of the density matrix $\rho$ are calculated by solving the Liouville equation with a previously described method.[12] The Fourier-transformed equations are solved in the Liouville space using the usual Green's functions encountered in the linear response theory. The time-dependent perturbation theory is used to the first order relative to the interaction with the optical field $\vec{E}_1$ (weak field). For the optical Hanle effect, the level shift is not due to a magnetic field as in the usual Hanle effect but is produced by a second intense optical field $\vec{E}_2$ (strong beam). The interaction with $\vec{E}_2$ is treated to all orders using a diagrammatic development which can be summed. The summation technique for the diagrams is different for the three-level system[12(b)] and for the two-level system.[12(a)] In addition, the electromagnetic fields are treated classically as monochromatic plane waves (semiclassical theory), the atom-field interaction is restricted to the electric-dipole term and the rotating wave approximation is made (nonresonant terms neglected). Furthermore as we consider an atomic beam experiment, the problems of Doppler shifts and broadening are eliminated and no velocity averaging is needed.

### A. Three-level system

The characteristics of the three-level system are illustrated in Fig. 3. The Bohr frequencies $\omega_{ab}$ and $\omega_{bc}$ corresponds to allowed electric-dipole transition so that the $a \leftrightarrow c$ transition is forbidden. The weak laser beam (laser 1, frequency $\omega_1$) is nearly resonant with the $b \leftrightarrow c$ transition ($\omega_1 \sim \omega_{bc}$) and the frequency $\omega_2$ of the strong beam (laser 2) is close to the atomic frequency $\omega_{ab}$. The two atomic frequencies $\omega_{ab}$ and $\omega_{bc}$ are supposed to be very different from one another. The geometry and polarizations are shown on Fig. 2 (Faraday geometry); the sublevels coupled by the two fields $\vec{E}_1$ and $\vec{E}_2$ are indicated in Fig. 3.

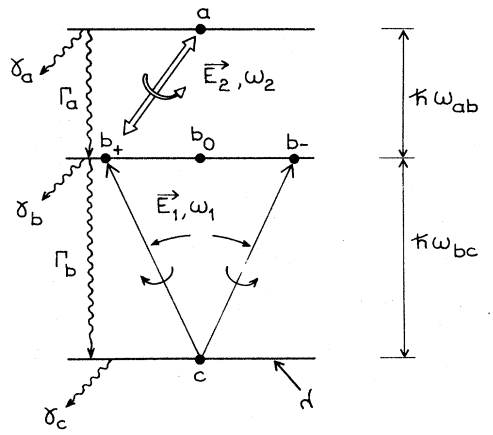


FIG. 3. Main characteristics of the simplified model used for the calculation of the optical Hanle effect in the three-level case. In the particular case shown on this figure no radiative decay out of the three-level system occurs. The closed system would correspond to $\gamma_a \to 0$, $\gamma_b \to 0$, $\gamma_c \to 0$, $\lambda \to 0$, and $\lambda/\gamma_c \to \rho_c^0$.

Without laser fields, the level $c$ is the only one populated. Let $\rho_c^0 = \lambda/\gamma_c$ be the corresponding population ($\lambda$ is the population-pumping rate for level $c$). The simplified model used for the relaxation of the three-level system includes spontaneous emission rates $\Gamma_i$ and collisional-relaxation rates $\gamma_i$ and $\gamma_{ij}$.

The steady-state solution, when the two laser fields are applied, gives for the coherence $\rho_{b_+b_-}$ the following expression:

$$\rho_{b_+b_-} = \frac{\rho_c^0 \beta_1^2}{G_{bb}^{-1}(0,0) - \beta_2^2 G_{ab}(0,1)} \left( \frac{1 + \beta_2^2 G_{ab}(0,1) G_{ac}(1,1)}{G_{bc}^{-1}(1,0) - \beta_2^2 G_{ac}(1,1)} + \frac{1}{G_{cb}^{-1}(-1,0)} \right), \tag{2}$$

$2\beta_1$ and $2\beta_2$ are the Rabi nutation frequencies corresponding, respectively, to the interaction with the two fields $2\beta_1 = d_{bc}E_1/\hbar$ and $2\beta_2 = d_{ab}E_2/\hbar$; $d_{ij}$ is the atomic dipole moment for the $i \leftrightarrow j$ transition.

$$G_{ij}(n_1, n_2) = (n_1\omega_1 + n_2\omega_2 - \omega_{ij} + i\Gamma_{ij})^{-1}, \tag{3}$$

$G_{ij}(n_1, n_2)$ is a linear response Green's function with $i, j = a, b, c$, $n_1, n_2 = 0, \pm 1$, $\Gamma_{ij} = \gamma_{ij} + \frac{1}{2}(\Gamma_i + \Gamma_j)$, $\gamma_{ij} \geq \frac{1}{2}(\gamma_i + \gamma_j)$, and $\Gamma_{ii} = \gamma_i + \Gamma_i$. $G_{ac}(1,1)$, for instance, is a typical two-photon term which can couple the levels $a$ and $c$ since $(\omega_1 + \omega_2) \sim \omega_{ac}$. However, the optical Hanle effect becomes meaningful only in the case of a large detuning $\delta_2 = \omega_2 - \omega_{ab}$ for the strong laser, i.e., under the conditions

$$|\delta_2| \gg \Gamma_{ii}, \Gamma_{ij}, \beta_i, \quad |\delta_1| = |\omega_1 - \omega_{bc}|. \tag{4}$$

These assumptions allows us to considerably simplify the expression (2). They correspond to the situation where the notion of radiative shift can be defined.

For the sake of simplicity we consider that we have a closed system where the relaxation rates $\gamma_i \to 0, \gamma_{ij} \to 0$ and the pumping rate $\lambda \to 0$, keeping $\lambda/\gamma_c$ constant and equal to $\rho_c^0$. We also assume that $\Gamma_c = 0$ ($c$ is a fundamental level). This leads

to the following simplified expression for the coherence $\rho_{b_+b_-}$:

$$\rho_{b_+b_-} = \frac{\beta_1^2\rho_c^0}{\Delta + i\Gamma_b}\left(\frac{1}{\delta_1 + \Delta + i\Gamma_b i\frac{1}{2}\Gamma_b} - \frac{1}{\delta_1 - i\Gamma_b - i\frac{1}{2}\Gamma_b}\right). \quad (5)$$

$\Delta = -\beta_2^2/\delta_2$ is the radiative shift induced by the strong beam. Consequently, the absorption and dispersion signals are given by

$$S_A = \beta_1^2\rho_c^0 \frac{2\delta_1(\delta_1+\Delta)+\frac{1}{2}\Gamma_b^2}{[\delta_1^2+\frac{1}{4}\Gamma_b^2][(\delta_1+\Delta)^2+\frac{1}{4}\Gamma_b^2]}, \quad (6)$$

$$S_D = \beta_1^2\rho_c^0 \frac{-\Delta\Gamma_b}{[\delta_1^2+\frac{1}{4}\Gamma_b^2][(\delta_1+\Delta)^2+\frac{1}{4}\Gamma_b^2]}. \quad (7)$$

The corresponding expression for the incoherent part of the fluorescence signal is

$$S_I = \rho_{b_+b_+} + \rho_{b_-b_-} = \beta_1^2\rho_c^0\left(\frac{1}{(\delta_1+\Delta)^2+\frac{1}{4}\Gamma_b^2} + \frac{1}{\delta_1^2+\frac{1}{4}\Gamma_b^2}\right), \quad (8)$$

so that we have $(S_I - S_A)/S_D = -\Delta/\Gamma_b$. A similar relation is obtained for the magnetic Hanle effect.[11] Considering the absorption and dispersion signals as a function of the distance between the shifted sublevels for a resonant excitation of the $b$ level ($\delta_1 = 0$) leads to

$$S_A = \frac{8\beta_1^2\rho_c^0}{\Gamma_b^2}\frac{1}{1+4y^2}, \quad S_D = \frac{8\beta_1^2\rho_c^0}{\Gamma_b^2}\frac{2y}{1+4y^2}, \quad (9)$$

with $y = -\Delta/\Gamma_b$.

The absorption-shaped $S_A$ and dispersion-shaped $S_D$ resonance curves are shown in Fig. 4 in the case $\delta_2 = 10\Gamma_b$; the curves calculated according to the exact formula (2) or to the simplified expressions (9) differ slightly but significantly. For a larger value of the detuning the approximation is fully justified and one can use the Lorentzian expressions (9). This is illustrated in Fig. 5(a) in the case $\delta_2 = 50\Gamma_b$.

Up to now we have considered the case of narrow-band (monochromatic) excitation. If the weak field is indeed provided by a broad-band source, the excitation will be kept resonant even when the strong beam is applied. A pure level-crossing effect is thus expected, just as for the magnetic Hanle effect, in the broad-band excita-

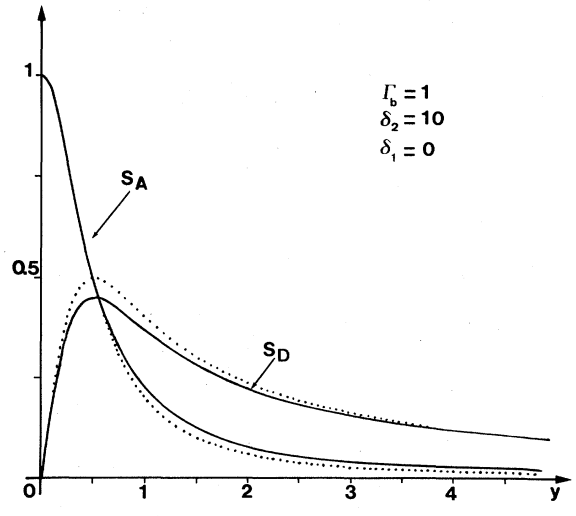


FIG. 4. $S_A$ and $S_D$ resonance curves versus the reduced variable $y = -\Delta/\Gamma_b$ in the three-level case ($\delta_2 = 10\Gamma_b$; $\delta_1 = 0$). Full line: Exact expression [Eq. (2)]. Dashed line: Simplified expression [Eq. (9)].

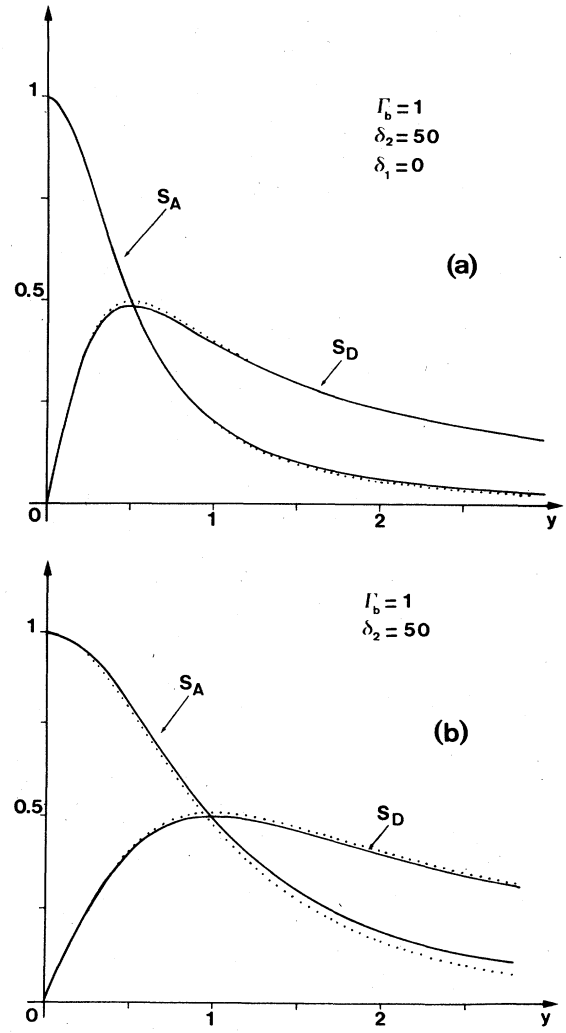


FIG. 5. $S_A$ and $S_D$ resonance curves versus the reduced variable $y = -\Delta/\Gamma_b$ in the three-level case ($\delta_2 = 50\Gamma_b$; $\delta_1 = 0$). (a) Narrow-band excitation. Full line: Exact expression [Eq. (2)]. Dashed line: Simplified expression [Eq. (9)]. (b) Broad-band excitation. Full line: Lorentzian curves of Eq. (10). Dashed line: Expressions (6) and (7) integrated over $\delta_1$ between $-20\Gamma_b$ and $+20\Gamma_b$.

tion regime. The resonance shapes are easily obtained after a summation over $\delta_1$ (from $-\infty$ to $+\infty$) of the expressions of $S_A$ and $S_D$ [Eqs. (6) and (7)]. This leads to

$$S_A \propto 1/(1+y^2), \quad S_D \propto y/(1+y^2), \quad y = -\Delta/\Gamma_b. \tag{10}$$

The same Lorentzian curves would have been obtained in the magnetic Hanle effect case, provided that the reduced variable is redefined to $y' = 2\Omega/\Gamma_b$ where $2\Omega$ is the Zeeman splitting of the $b_+$ and $b_-$ sublevels [Fig. 1(a)]. Figure 5(b) shows the curves corresponding to (10) together with the corresponding curves obtained after integration of (6) and (7) over a limited range of $\delta_1$ values.

In the case of three-level systems the broad-band excitation [Eq. (10)] as well as the narrow-band excitation [Eq. (8)] gives Lorentzian shapes for the optical Hanle effect but the width is reduced by a factor of 2 in the narrow-band case; this is illustrated in Fig. 5.

Let us remark now that, in the case of linear polarizations at 45° from one another for the two beams (Kerr geometry),[6(b)] the expression for the Hertzian coherence $\rho_{b_+b_0}$ would be given by the same expression as $\rho_{b_+b_-}$ in the present case (Faraday geometry), i.e., by (2) or (5).

### B. Two-level system (Fig. 6)

The geometry and the polarizations are the same as in the three-level case (Fig. 2) but now the frequencies of both laser beams lie in the vicinity of the atomic frequency $\omega_{bc}$. The sublevels coupled by the two fields are indicated in Fig. 6. The notation for the relaxation and pumping rates are the same as previously; without laser beams the upper level $b$ is not populated. An important point is that now the strong beam acts upon the $c$ level and can shift the position of this level as well as that of the $b_-$ level.

When the two laser fields are turned on, one finds for the expression of the coherence term $\rho_{b_+b_-}$ under steady-state regime

$$\rho_{b_+b_-} = \frac{\beta_1^2\rho_c^0}{[G_{bb}^{-1}(0,0) - \beta_2^2 G_{bc}(0,1)](\det X_2)}\left(X_1 - \beta_2^2 G_{bb}(0,0)X_2 + \frac{\beta_2^2 G_{bb}(1,-1)[Z_2 - \beta_2^2 G_{bb}(0,0)G_{bc}(1,0)X_2]}{[G_{bc}^{-1}(1,0) - \beta_2^2 G_{bb}(1,-1)]} - \frac{\beta_2^2 Z_2^*[G_{bb}(-1,+1)G_{cb}(-1,0) + G_{cc}(1,-1)Z_2]}{(\det Y^*)}\right), \tag{11}$$

with

$$\begin{aligned} X_1 &= G_{bc}(1,0) + G_{cb}(-1,0), \\ X_2 &= G_{bc}(0,1) + G_{cb}(0,-1), \\ Z_2 &= G_{bc}(1,0) + G_{cb}(0,-1), \\ Y^* &= G_{bc}(-1,2) + G_{cb}(-1,0), \\ \det X_2 &= 1 - \beta_2^2[G_{bb}(0,0) + G_{cc}(0,0) - g_{cb}(0,0)]X_2, \\ \det Y^* &= 1 - \beta_2^2[G_{bb}(-1,1) + G_{cc}(-1,1) - g_{cb}(-1,1)]Y^*. \end{aligned} \tag{12}$$

$G_{ij}(n_1, n_2)$ has been defined previously through Eq. (3) with, in the particular case, $n_1, n_2 = 0, \pm 1, \pm 2$; $2\beta_2 = d_{bc}E_2/\hbar$ is the Rabi frequency for the strong beam and the term $g_{cb}(n_1, n_2) = i\Gamma_b G_{cc}(n_1, n_2)G_{bb}(n_1, n_2)$ is due to the spontaneous emission rate from $b$ to $c$.

Just as in the three-level case, the above expressions become much more simple and significant in the situation of large detunings for the strong beam (4). This approximation leads to a reduction of the saturation term ($\det X_2 \sim 1$) and shows the fundamental importance of the two-photon terms $[G_{bc}^{-1}(1,0) - \beta_2^2 G_{bb}(1,-1)]$ and $\det Y^*$ from which the radiative shift occur.

The following expressions will be given for a closed system considering only the spontaneous emission terms from $b$ to $c$ in the relaxation matrix; this corresponds closely to the experimental situation of Sec. III. Thus we have to make $\gamma_i \to 0$ and $\lambda \to 0$ while keeping $\gamma_b/\gamma_c = 1$ and $\lambda/\gamma_c = \rho_c^0$.

Provided (4) is valid, one obtains

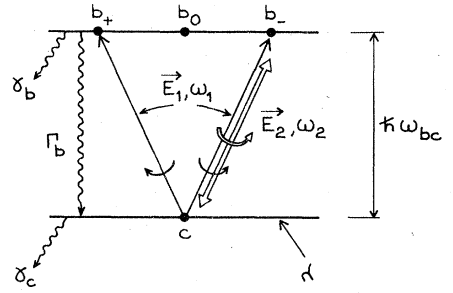


FIG. 6. Main characteristics of the model used for the calculation of the optical Hanle effect in the two-level case.

$$\rho_{b+b-} = \frac{\beta_1^2\rho_c^0}{G_{bb}^{-1}(0,0)-\beta_2^2 G_{bc}(0,1)}\left(\frac{1}{G_{bc}^{-1}(1,0)-\beta_2^2 G_{bb}(1,-1)} + \frac{1}{G_{cb}^{-1}(-1,0)-\beta_2^2[G_{bb}(-1,1)+G_{cc}(-1,1)-g_{cb}(-1,1)]}\right)$$

$$= \frac{\beta_1^2\rho_c^0}{\Delta + i\Gamma_b}\left(\frac{1}{\delta_1 - \Delta + i\frac{1}{2}\Gamma_b} - \frac{1}{\delta_1 - 2\Delta - i\frac{1}{2}\Gamma_b}\right). \tag{13}$$

The expressions for $S_A$ and $S_D$ are now

$$S_A = \beta_1^2\rho_c^0 \frac{2\delta_1(\delta_1 - 3\Delta) + 4\Delta^2 + \frac{1}{2}\Gamma_b^2}{[(\delta_1-\Delta)^2 + \frac{1}{4}\Gamma_b^2][(\delta_1 - 2\Delta)^2 + \frac{1}{4}\Gamma_b^2]},$$

$$S_D = \beta_1^2\rho_c^0 \frac{-\Delta\Gamma_b}{[(\delta_1-\Delta)^2 + \frac{1}{4}\Gamma_b^2][(\delta_1 - 2\Delta)^2 + \frac{1}{4}\Gamma_b^2]}. \tag{14}$$

When the excitation by the weak field is resonant ($\delta_1 = 0$), one obtains

$$S_A = \frac{8\beta_1^2\rho_0^c}{\Gamma_b^2}\frac{1+8y^2}{(1+4y^2)(1+16y^2)},$$

$$S_D = \frac{8\beta_1^2\rho_0^c}{\Gamma_b^2}\frac{2y}{(1+4y^2)(1+16y^2)}, \tag{15}$$

$$y = -\Delta/\Gamma_b.$$

The absorption-shaped $S_A$ and the dispersion-shaped $S_D$ resonance curves are shown in Figs. 7 and 8(a). As in the three-level case, a comparison is made between the results obtained with the exact equation (11) and with Eq. (15).

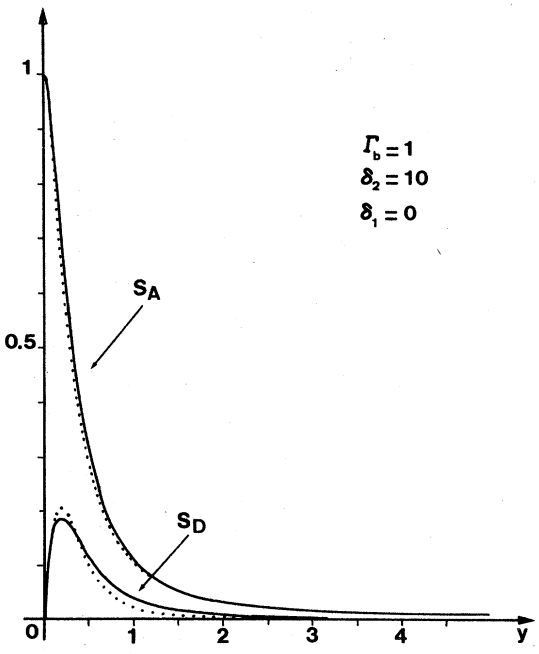


FIG. 7. $S_A$ and $S_D$ resonance curves versus the reduced variable $y = -\Delta/\Gamma_b$ in the two-level case ($\delta_2 = 10\Gamma_b$; $\delta_1 = 0$). Full line: Exact expression [Eq. (11)]. Dashed line: Simplified expression [Eq. (15)].

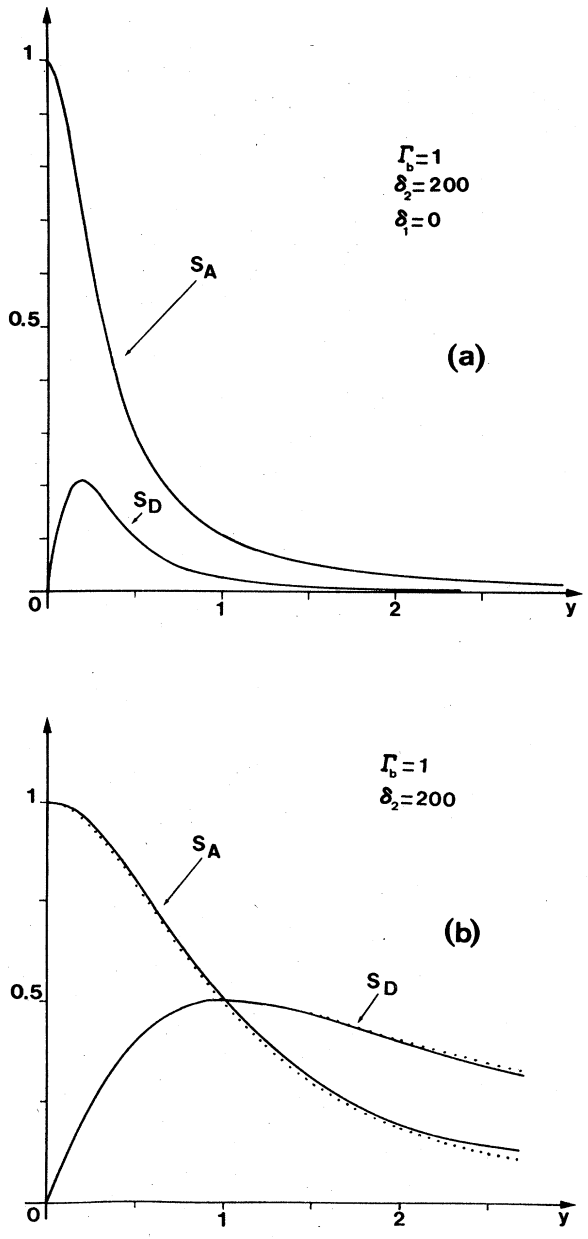


FIG. 8. $S_A$ and $S_D$ resonance curves versus the reduced variable $y = -\Delta/\Gamma_b$ in the two-level case ($\delta_2 = 200\Gamma_b$, $\delta_1 = 0$). (a) Narrow-band excitation. The curves corresponding to the exact expressions [Eq. (11)] or to the approximation of Eq. (15) cannot be distinguished. (b) Broad-band excitation. Full line: Lorentzian curves [Eq. (10)]. Dashed line: Expression (14) integrated over $\delta_1$ between $-50\Gamma_b$ and $+50\Gamma_b$.

In the case $\delta_2 = 200\Gamma_b$ [Fig. 8(a)], the corresponding curves are not separated.

The line shapes are quite different from that obtained in the three-level case: The width is reduced as well as the relative amplitude of the dispersion curve.

Just as for three-level systems one can consider the case of broad-band excitation for two-level systems. Integrating Eq. (14) over $\delta_1$ from $-\infty$ to $+\infty$ gives exactly the same Lorentzian shapes as previously [Eq. (10)]; this is illustrated on Fig. 8(b). Figures 8(a) and 8(b) also allow a comparison between the narrow-band case and the broad-band case for the optical Hanle effect in a two-level system.

### C. Discussion

In order to discuss the particularities of the optical Hanle effect (Faraday geometry), let us briefly recall the expression of the coherence term $\rho_{b_+b_-}$ in the case of the usual magnetic Hanle effect in the $J=0 \rightarrow J=1$ transition of concern [Fig. 1(a)]:

$$\rho_{b_+b_-} = \begin{cases} \beta_1^2 \rho_c^0 \dfrac{1}{G_{b_+b_-}^{-1}(0)} \left( \dfrac{1}{G_{b_+c}^{-1}(1)} + \dfrac{1}{G_{cb_-}^{-1}(-1)} \right), \\ \beta_1^2 \rho_c^0 \dfrac{1}{-2\Omega + i\Gamma_b} \left( \dfrac{1}{(\delta_1 - \Omega) + i\frac{1}{2}\Gamma_b} - \dfrac{1}{(\delta_1 + \Omega) - i\frac{1}{2}\Gamma_b} \right), \end{cases} \tag{16}$$

where $\Omega = g\mu_B H$ is the Zeeman shift.

The above expression as well as the corresponding ones [Eqs. (5) and (13)] for the optical Hanle effect can be written in the same form:

$$\rho_{b_+b_-} = (1/C)(1/B_+ - 1/B_-).$$

Let us discuss the different terms, having in mind the different situations illustrated in Fig. 1.

(a) $C$ is a resonant denominator which represents the pure level crossing term; it contains the energy difference between the $b_-$ and $b_+$ sublevels which is equal to the following:

(i) $-2\Omega$ in the usual magnetic Hanle effect.

(ii) $\Delta$ in the optical Hanle effect for which only one sublevel is shifted ($b_+$ in the three-level case and $b_-$ in the two-level case).

(b) $B_+$ is a resonant denominator corresponding to the excitation of the $c \rightarrow b_+$ transition. The energy of this transition is shifted from its zero-field value. The shift is as follows:

(i) $\Omega$ (Zeeman shift of $b_+$) in the usual magnetic Hanle effect.

(ii) $-\Delta$ (light shift of $b_+$) in the optical Hanle effect (three-level case).

(iii) $\Delta$ (light shift of the lower level $c$ of $-\Delta$) in the optical Hanle effect (two-level case).

(c) $B_-$ is a resonant denominator corresponding to the excitation of the $c \rightarrow b_-$ transition. The energy of this transition is shifted from its zero-field value. The shift is as follows:

(i) $-\Omega$ (Zeeman shift of $b_-$) in the usual magnetic Hanle effect.

(ii) zero (no radiative shift for $b_-$) in the optical Hanle effect (three-level case).

(iii) $2\Delta$ (light shift $\Delta$ for $b_-$ and $-\Delta$ for $c$) in the optical Hanle effect (two-level case).

Let us remark that the radiative shift $\Delta$ is positive or negative according to the fact that the detuning is negative or positive.

## III. EXPERIMENTAL INVESTIGATION OF THE OPTICAL HANLE EFFECT

### A. Experimental arrangement

We have not found any suitable three-level system for the investigation of the optical Hanle effect and we had to turn to a two-level experiment. The experiment has been performed with the barium resonance transition at 553.5 nm ($6s^2\,{}^1S_0 \rightarrow 6s6p\,{}^1P_1$) using a highly collimated atomic beam.

Let us briefly outline the main characteristics of the experiment; the experimental setup has been described with some detail in a previous paper.[13] The geometry and polarizations are that of Fig. 2; the Ba atomic beam is crossed at a right angle by two counter-propagating laser beams; the weak beam is frequency locked to the $^{138}$Ba line and the strong beam is detuned in the range $-750$– $-6000$ MHz from the same line (the natural width is $\Gamma_b = 19$ MHz). The polarization direction of the weak beam is rotated at frequency $\nu$ and the part of the fluorescence modulated at $2\nu$ is detected thus giving, directly, $S_A$ (in-phase signal) and $S_D$ (in-quadrature signal).[11] The resonance signals $S_A$ and $S_D$ are directly recorded versus the strong-beam power for various values of the detuning. In order to get the so-called "broad-band excitation" experimental curves, we have used a large amplitude for the frequency modulation of the weak laser beam.[14]

Let us now discuss some particular points which correspond to some limitations of our experiment. First, we had to work with natural barium which includes about 28% of undesirable isotopes. However, under our polarization conditions, the $^{138}$Ba line is much more intense than the eight other lines which are all located on the high-frequency side.[15] The weak beam is locked to the $^{138}$Ba line; to avoid spurious effects due to the other isotopes, negative values of the detuning $\delta_2$ have been used in our experiment. This pre-

vents the direct pumping of the other isotopes by the strong beam and, as the light shifts are positive, the shifted transition frequencies for the undesirable isotopes cannot be brought into resonance with the weak beam. Another point is that we used nonuniform beams. The Gaussian distribution of the intensities in the beams and the fact that the weak-beam size was not very much smaller that the strong-beam size led to a deformation of the resonance curve which had to be included in the fit of the experimental curves.

Other parasitic effects such as nonzero residual Doppler width, optical pumping effects due to the $^1P_1 - {}^1D_2$ transition, spurious diffused laser light, and fluorescence light not produced in the interaction region—should be considered. Indeed, we have found that the relevant consequences on the resonance shape were not very important and that they do not need to be included in the fitting procedure.

### B. Experimental results

The experimental curves $S_A$ and $S_D$ corresponding to the case of narrow-band excitation are shown in Fig. 9. These resonance curves have been obtained versus the strong-beam power and for frequency detunings ranging from $-750$ to $-6000$ MHz. The line shape is expected to be a function of the optical light shift $\Delta = -\beta_2^2/\delta_2$; $\beta_2^2$ is proportional to the power density $P_L$. The $S_A$ and $S_D$ curves obtained for different values of the strong-beam detuning $\delta_2$ should have exactly the same shape when plotted versus the variable $P_L/\delta_2$. This $1/\delta_2$ scaling law has been successfully checked for the whole set of experimental curves (Fig. 9). In Fig. 9 for $P_L = P_0 \simeq 35$ W/cm$^2$, the light shift $\Delta$ is about 17 MHz and the reduced variable $y = \Delta/\Gamma_b \simeq 0.91$.

The experimental curves corresponding to the so-called "broad-band" excitation case are shown in Fig. 10. For these resonance curves, we have also checked the $1/\delta_2$ scaling law (Fig. 10). In Fig. 10, for $P_L = P_0 \simeq 35$ W/cm$^2$, the light shift $\Delta$ is about 46 MHz and the reduced variable $y = \Delta/\Gamma_b \simeq 2.43$.

As far as the position of the maximum of the dispersion-shaped resonance curve and the relative amplitude of $S_A$ and $S_D$ curves are concerned, the experimental curves qualitatively behave as expected. The maximum of the narrow-band excitation curve is obtained for a light-shift value much smaller than the natural width and, for the broad-band case, this maximum is shifted towards the higher values of the light shift. The relative amplitude of the dispersion curve is much smaller in the case of narrow-band excitation than in the case of broad-band excitation.

We have tried to fit directly the narrow-band experimental curves using Eq. (15). We have found that this could not be done in a satisfactory way and we have tried to introduce corrections to the theoretical line shape in order to take into

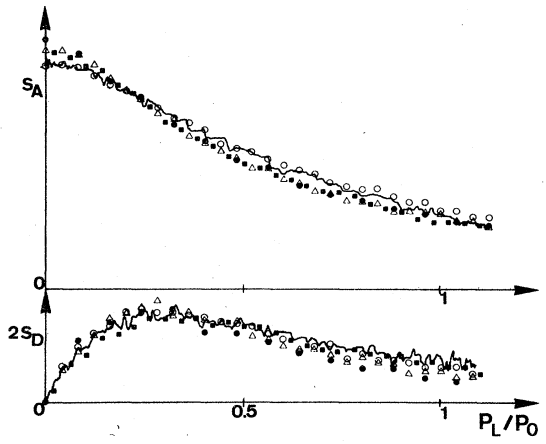


FIG. 9. Experimental resonance curves $S_A$ and $S_D$ for narrow-band excitation. The reference curves (solid line) are relative to the detuning value $\delta_2^0 = -6000$ MHz; the other experimental curves (detuning $\delta_2$) are plotted with a power scale divided by the factor $\delta_2^0/\delta_2$ for $\delta_2 = -750$ MHz (●); $-1500$ MHz (△); $-3000$ MHz (■); $-4500$ MHz (○). The power density of the strong beam $P_L$ is given in the $P_0$ unit ($P_0 \simeq 35$ W/cm$^2$).

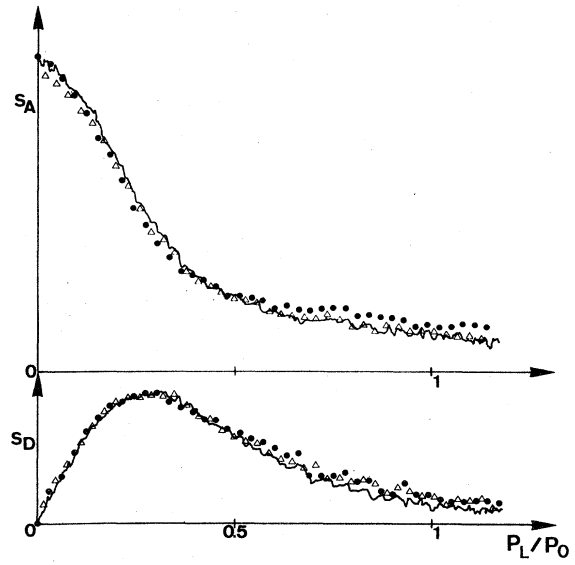


FIG. 10. Experimental resonance curves $S_A$ and $S_D$ for broad-band excitation. The reference curves (solid line) are relative to the detuning value $\delta_2^0 = -2250$ MHz; the other experimental curves (detuning $\delta_2$) are plotted with a power scale divided by the factor $\delta_2^0/\delta_2$ for $\delta_2 = -750$ MHz (●); $-1500$ MHz (△). The power density of the strong beam $P_L$ is given in the $P_0$ unit ($P_0 \simeq 35$ W/cm$^2$).

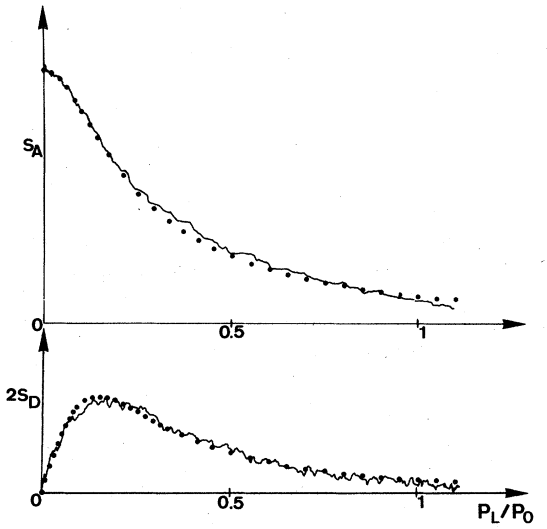


FIG. 11. Theoretical fit of the narrow-band excitation curves $S_A$ and $S_D$. The experimental curves (solid line) correspond to $\delta_2 = -3000$ MHz and the corresponding calculated curve (dotted line) is obtained for $P_0 = 35$ W/cm$^2$ (i.e., $y = 1.81$ for $P_L = P_0$), and for a ratio of two between the strong- and weak-beam areas.

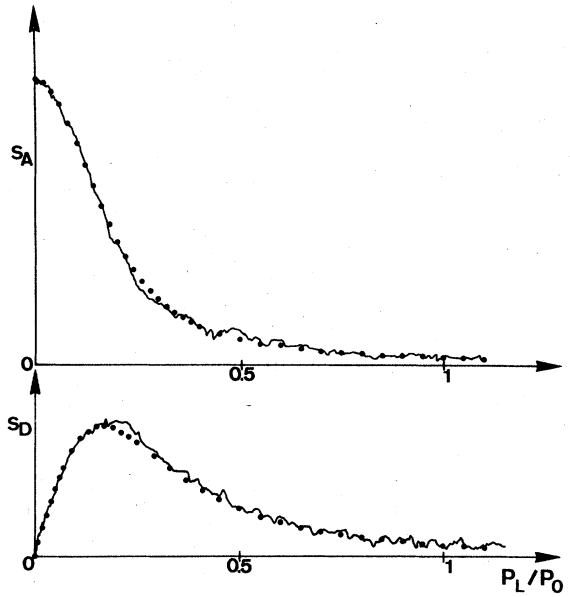


FIG. 12. Theoretical fit of the broad-band excitation curves $S_A$ and $S_D$. The experimental curves (solid line) correspond to $\delta_2 = -1500$ MHz and the corresponding calculated curve (dotted line) is obtained for $P_0 = 40$ W/cm$^2$ (i.e., $y = 4.19$ for $P_L = P_0$).

account some experimental limitations. We have found that we had to introduce the Gaussian distribution of the beam intensities in order to reproduce the recorded line shapes. Taking into account this correction, we have been able to fit the *whole* set of experimental curves using the following adjustable parameters:

A scaling parameter $P_0$ for the laser power axis; this parameter has the *same value* for all the curves to be fitted.

A normalization parameter of the amplitudes for each ensemble of $S_A$ and $S_D$ curves (i.e., for each value of $\delta_2$ used in the experiment); in addition, for each $S_A$ curve, a background is introduced which accounts for spurious light coming from scattered laser light or unwanted fluorescence.

The result of this fitting procedure is illustrated in Fig. 11 for a particular set of $S_A$ and $S_D$ curves; the agreement between the calculated and the experimental curve is good. The optimized value of $P_0$ is in close agreement with the corresponding value deduced from another experiment where the Autler-Townes doublet produced by the strong beam at resonance has been observed.[16]

The corresponding fit for the broad-band excitation curve could not be obtained in such a satisfactory way. The amplitude of the frequency modulation in this case was certainly not large enough to produce a real broad-band excitation so that the recorded curves are not Lorentzian shaped. One can account in an effective way for the weak laser linewidth under two different ways. On one hand, one can make a summation over $\delta_1$ in the range $(-\frac{1}{2}\Gamma_{\text{eff}}, +\frac{1}{2}\Gamma_{\text{eff}})$ of Eq. (13) to get the theoretical line shape. On the other hand, one can introduce directly an effective width $\frac{1}{2}\Gamma_{\text{eff}}$ instead of $\frac{1}{2}\Gamma_b$ in the second term of (13), which contains the resonant character of the excitation of the $b_+$ and $b_-$ sublevels (see Sec. II C).

The latter case which corresponds to the introduction of a Lorentzian shape for the laser spectrum is much better suited to computer optimizations. The resulting line shape was found to be almost the same in both cases for our parameter values. We have also checked that, in this particular case, the Gaussian distribution of intensities had a rather small influence upon the line shape. The final fit was thus obtained by adding a $\Gamma_{\text{eff}}$ parameter to the list of parameters used in the previous fit. The results are illustrated in Fig. 12; the optimized parameter $\Gamma_{\text{eff}}$ was about 100 MHz. We had estimated the amplitude of the frequency modulation to be somewhat greater than this value. Indeed, a true broad-band excitation regime could be obtained using a Ba hollow cathode source and/or taking advantage of Doppler broadening in a vapor.

*Laboratoire associé à l'Université Paris-Sud.
[1]W. Hanle, Z. Phys. 30, 93 (1924).
[2]A. Mitchell and M. Zemansky, *Resonance Radiation and Excited Atoms* (Cambridge University Press, Cambridge, 1961).
[3]B. Decomps, M. Dumont, and M. Ducloy, in *Topics in Applied Physics*, edited by H. Walther (Springer, Berlin, 1976), Vol. 2.
[4]C. Cohen-Tannoudji, in *Frontiers in Laser Spectroscopy, Les Houches, 1975*, edited by R. Balian, S. Haroche, and S. Liberman (North-Holland, Amsterdam, 1976).
[5]W. Hanle, Z. Phys. 35, 346 (1926).
[6](a) V. P. Kaftandjian and L. Klein, Phys. Lett. 62A, 317 (1977); (b) V. P. Kaftandjian, L. Klein, and W. Hanle, Phys. Lett. 65A, 188 (1978).
[7]C. Delsart, J.-C. Keller, and V. P. Kaftandjian, in *Laser Spectroscopy IV*, edited by H. Walther and K. W. Rothe (Springer, Berlin, 1979), p. 618.
[8]P. F. Liao and J. E. Bjorkholm, Opt. Commun. 16, 392 (1976); C. Cohen-Tannoudji, Metrologia 13, 161 (1977); and references therein.
[9]C Wieman and T. W. Hänsch, Phys. Rev. Lett. 36, 1170 (1976); J.-C. Keller and C. Delsart, Opt. Commun. 20, 147 (1977); C. Delsart and J.-C. Keller, J. Appl. Phys. 49, 3662 (1978).
[10]V. P. Kaftandjian, B. Talin, and L. Klein, J. Phys. (Paris) 40, 1037 (1979).
[11]D. Lecler, R. Ostermann, W. Lange, and J. Luther, J. Phys. (Paris) 36, 647 (1975).
[12](a) A. Ben-Reuven and L. Klein, Phys. Rev. A 4, 753 (1971); (b) L. Klein, M. Giraud, and A. Ben-Reuven, *ibid.* 10, 682 (1974).
[13]C. Delsart, J.-C. Keller, and V. P. Kaftandjian, Opt. Commun. 32, 406 (1980).
[14]H. Brand, W. Lange, J. Luther, and B. Nottbeck, Opt. Commun. 13, 286 (1975).
[15]P. E. G. Baird, R. J. Brambley, K. Burnett, D. N. Stacey, D. M. Warrington, and G. K. Woodgate, Proc. R. Soc. London Ser. A 365, 567 (1979).
[16]C. Delsart, J.-C. Keller, and V. P. Kaftandjian (unpublished).